Dielectric function of epitaxial quasi-freestanding monolayer graphene on Si-face 6H-SiC in a broad spectral range

Kristupas Kazimieras Tikuišis,[1] Adam Dubroka,[2] Klára Uhlířová,[1] Florian Speck,[3] Thomas Seyller,[3] Maria Losurdo,[4] Milan Orlita,[5] and Martin Veis[1,*]

[1]*Faculty of Mathematics and Physics, Charles University, Ke Karlovu 2027/3, 121 16 Prague 2, Czech Republic*
[2]*Department of Condensed Matter Physics, Faculty of Science, Masaryk University, Kotlářská 2, 611 37 Brno, Czech Republic*
[3]*Institut für Physik, Technische Universität Chemnitz, Reichenhainer Strasse 70, 09126 Chemnitz, Germany*
[4]*Institute of Nanotechnology, CNR-NANOTEC, Via Orabona 4, 70126 Bari, Italy*
[5]*Laboratoire National des Champs Magnétiques Intenses Grenoble-CNRS, 25 Martyrs Avenue, BP 166, 38042 Grenoble Cedex 9, France*

(Received 18 November 2022; revised 22 February 2023; accepted 20 March 2023; published 17 April 2023)

We present a study of the optical properties of quasi-freestanding epitaxial monolayer graphene grown on the Si face of 6H-SiC (0001) in a broad spectral range from midinfrared to ultraviolet. After growth, the sample was intercalated by hydrogen in order to ensure that no dangling bonds between the substrate and graphene layer remain. Spectral dependence of the dielectric function of graphene was parametrized based on spectroscopic ellipsometry fits. We show that, from the viewpoint of optical properties, the investigated sample is very close to exfoliated graphene. We provide information about the spectral dependence of the complex dielectric function of quasi-freestanding graphene in a broad spectral range.

DOI: 10.1103/PhysRevMaterials.7.044201

I. INTRODUCTION

As the current electronics industry is approaching its limits in terms of speed, size, and bandwidth, graphene stands as a solid candidate for the basis of next-generation devices. Its most alluring properties are a high electron mobility surpassing 10 000 $cm^2\,V^{-1}\,s^{-1}$ (or even tenfold higher in suspended graphene devices or graphene placed on h-BN) [1–3], carrier density tuning by an external electric field [1,4], pico- and femtosecond timescales of carrier heating and cooling [5], etc. Graphene can be used as a transparent electrode enhancing the effectiveness of transparent conductors for future flexible devices [6,7] or power conversion efficiency for solar cells [8].

Exfoliation delivers the highest-quality samples [9–12] but only small footprints of material can be produced in this way. Chemical vapor deposition (CVD) allows growing graphene multilayers on various surfaces [13–15] but sometimes requires additional steps to transfer graphene from the growth substrate to the application substrate. In this regard, graphitization of the top layers of silicon carbide by annealing is an easy and cheap shortcut to help pass these limitations for the mass production of multi- and especially monolayers. The lowest graphitized layer is covalently bonded to the substrate surface. The bonding reduces the electron mobility and does not allow linear dispersion to develop. Furthermore, the chemical potential strongly depends on temperature, most probably due to strong substrate-graphene phonon coupling [16]. Intercalation by hydrogen is an already proven method to suppress these bonds and produce the so-called quasi-freestanding monolayers having all of the graphene properties [17]. In order to utilize graphene in the industrial mass production of multilayered devices as transparent electrodes, it is convenient to know its optical properties in the broadest spectral range possible.

Graphitization is faster on the C face but it also makes it difficult to ensure the growth of a single layer as usually multilayers are grown. Graphitization is slower and easier to control on the Si face [18]. To the best of our knowledge, previous spectroscopic ellipsometry studies on graphene were focused on 3C-SiC and 4H-SiC allotropes [19–22]. There are only a few reports presenting optical properties of graphene grown on 6H-SiC in a limited spectral range [21,23]. 6H-SiC is widely used in commercial device fabrication and could serve as the basis for graphene-based circuits and optoelectronic devices. Hence we report on an optical examination of a quasi-freestanding monolayer graphene obtained by the intercalation of Si-face 6H-SiC. Yet we show that its optical properties compete with those of the best-quality exfoliated graphene, namely in terms of the sharpness of the exciton peak and the overall infrared (IR) response.

II. EXPERIMENT DETAILS

The investigated epitaxial quasi-freestanding monolayer graphene sample was prepared by annealing of 0.5-nm-thick Si-face 6H-SiC at a graphitization temperature of 1450 °C and argon atmosphere. The quasi-freestanding graphene layer was obtained by hydrogen intercalation of a single layer of 6H-Si (0001). The surface quality and morphology were measured by atomic force microscopy (AFM). Optical properties were investigated using a combination of Woollam's spectroscopic ellipsometers RC2 and V-VASE in order to cover a broad spectral range. The RC2 ellipsometer allowed us to measure

*veis@karlov.mff.cuni.cz

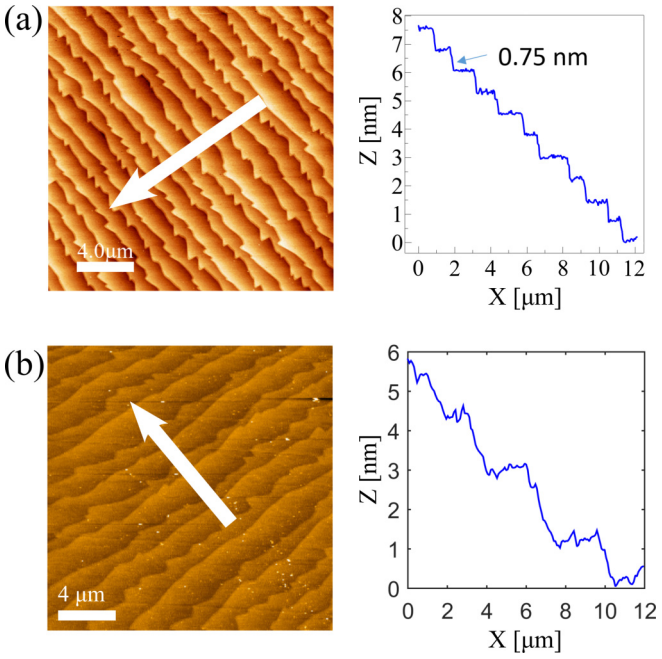

FIG. 1. False color two-dimensional (2D) AFM scan maps and selected profiles of the (a) intercalated reference SiC sample and (b) substrate+graphene sample. Only single profiles along the directions of the white arrows are shown for brevity. In (b), horizontal lines correspond to measurement artifacts. This complicated the baseline correction, distorting vertical distances in the subset on the right. To evaluate the precise average terrace height, raw uncorrected data at multiple spots were analyzed.

the Mueller matrix ellipsometry and unpolarized transmission data in the range from 0.7 to 5.5 eV. The transmission data served as an additional input allowing us to account for the features near the SiC band gap such as the absorption edge, absorption tail, etc. The V-VASE ellipsometer allowed us to acquire experimental data in the IR region down to 0.150 eV. All measurements were performed at room temperature under several angles of incidence ranging from 45° to 75°. The light beam diameter was approximately 3 mm, yielding the average optical response from such an area. Woollam's COMPLETEEASE software was used for advanced data processing. Obtained optical properties were compared to CVD-grown graphene on silicon using a standard approach.

III. SiC AND GRAPHITIZED SiC SURFACE MORPHOLOGY MEASUREMENTS

According to AFM measurements, the average width and height of SiC terraces of both the sample and reference right after cleaving and an initial hydrogen etching is 1.243 μm and 0.75 nm [half unit cell; Fig. 1(a)]. This is caused by surface orientation not matching the nominally on-axis oriented SiC wafers. Typical step heights are 1 or 0.5 of a 6H unit cell [24]. It indicates a miscut angle of 0.03°–0.04°. Graphitization at temperatures above 1200 °C promotes an additional microscopic surface restructuring, forming more steps. These steps tend to bunch together, and terraces become wider and higher on average. The final terrace morphology thus changes. Step bunching is a well-known phenomenon [21,24,25]. The sample surface area was about 5×5 mm, and in order to ensure statistically reliable surface morphology data of the graphitized hydrogen-intercalated sample, we have performed AFM measurements on five different places on the sample, each 20×20 μm: one in the center and the other four at every corner. The height of the terraces was estimated along the horizontal scanning direction so that any possible sample drift artifacts would be eliminated. According to the data, terraces became 1.4 nm high and 1.8 μm wide on average after bunching [Fig. 1(b)]. The terrace height was used as one of the input parameters for the ellipsometric data processing.

IV. SPECTROSCOPIC ELLIPSOMETRY DATA ANALYSIS

A reference bare SiC substrate and a graphitized sample, both prepared under the same conditions, were investigated. Prior to the graphitized sample, the optical properties of the bare substrate were characterized. Its optical response was then used as an input when fitting the data set obtained on the graphitized sample. This decreased the set of parameters to be fit at once.

The reference SiC substrate was modeled as a bulk birefringent material. Its ordinary and extraordinary axes were modeled independently. Its permittivity was described by a sum of oscillators fulfilling the Kramers-Kronig relations. All substrate oscillators were chosen to be of Cody-Lorentz type as it allows modeling a broad Lorentzian line shape with zero absorption below a defined absorption edge energy E_g. Several independent oscillators were required for each optical axis. The optical absorption edge energy parameter E_g was shared among all of them. The fitting procedure used all of the experimental data (ellipsometric quantities Ψ and Δ at multiple angles of incidence and IR optical transmission) simultaneously, resulting in the best set of oscillator parameters (amplitudes, energies, and broadenings). The resulting permittivity follows the spectral trends reported in other studies on 6H-SiC [26–31], and the absorption edge energy fitted to 2.93 eV.

Because the SiC substrate was polished from both sides and is transparent in almost the entire measured spectral range, backreflections from the back side of the substrate were observed, thus complicating data processing. The combination of the uniaxial anisotropy and reflections from the backside of the SiC substrate is responsible for the interference pattern below the SiC band gap. This is also visible in the graphene sample—see Figs. 2(a) and 2(b).

The thicknesses of the surface terrace steps in all investigated samples estimated by the AFM measurement were in the order of several nm, much lower than the wavelength of the probing radiation. Light is thus unable to distinguish the exact structure of layers so thin. The terraces are hence treated as a separate surface roughness layer on top of the sample. It uses the Bruggemann effective medium approximation (EMA) to describe the mixing of the optical response of the surrounding materials. It was composed of 50% air and 50% underlying SiC. Its initial thickness was set to the step height as measured by the AFM. A reasonable fit was achieved and the interference pattern in the spectra of ellipsometeric parameters was reproduced well (not shown here).

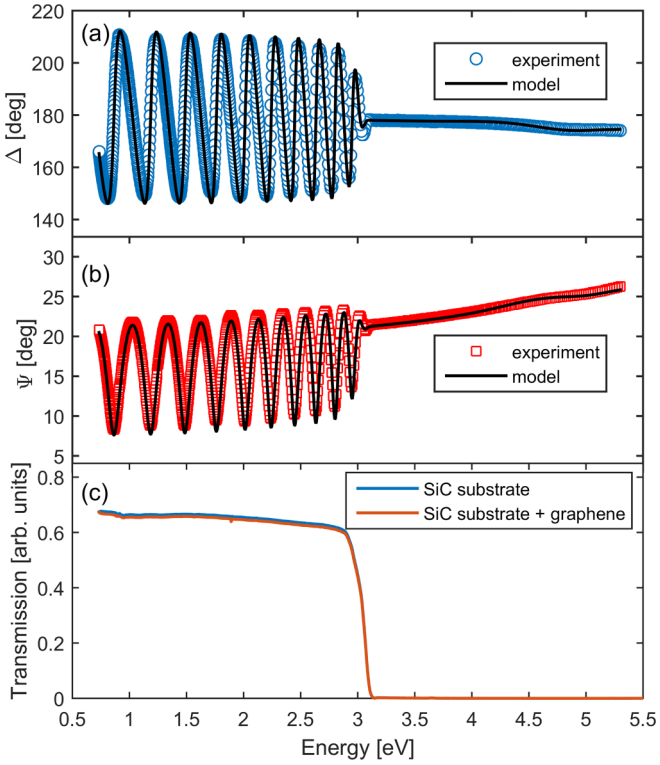

FIG. 2. Comparison of experimental data and modeled spectra of the SiC substrate and graphene at 55° of incidence. The main ellipsometric angles (a) Δ and (b) Ψ are provided. They exhibit oscillations induced by backside reflections. (c) Transmission data of SiC substrate and SiC substrate+graphene sample.

Several model structures have been proposed to describe the graphene sample. The thickness of monolayer graphene is taken as an interlayer spacing in graphite, e.g., 0.35 nm. In this case, it is much smaller than the height of the terrace steps (1.4 nm). We have evaluated various approaches to model the sample structure and to best fit the experimental data. The simplest models treated the structure as stratified layers of substrate and graphene with a potential additional surface roughness component. These approaches failed to deliver physically meaningful optical properties or did not fit to realistic layer thicknesses. Similar results and numerically unstable fits were obtained for more complicated model structures consisting of substrate, void layer, and graphene, which are supposed to reflect the terrace structure of the top layers.

Due to the atomic thickness of graphene and low terrace height, the light experiences an averaged refractive index of all involved materials at the surface. To maximally reflect the graphene layer structure with thin terrace steps, we have chosen a model structure consisting of the SiC substrate covered with a Bruggemann EMA layer composed of three materials, the underlying SiC, graphene, and air, as depicted in Fig. 3. The inclusion of air reflects the surface roughness. The optical properties of this layer are adjusted via the volume ratios of its components. The volume ratios of graphene, v_{graphene}, and interpenetrating air/substrate, v_{air} and $v_{\text{substrate}}$, range from 0% to 100% and are coupled. For low terrace angles they can be related to the total thickness t_{total} (in nm) of the top layer in

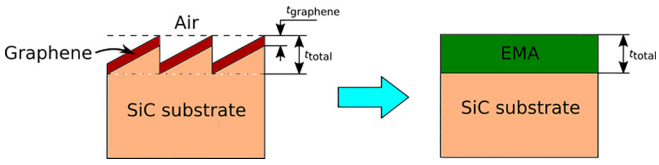

FIG. 3. Schematic sketch of the chosen model structure used for the parametrization of the optical properties of the graphene layer.

the following way:

$$v_{\text{graphene}} + v_{\text{air}} + v_{\text{substrate}} = 100\%. \tag{1}$$

The air and substrate filling factors/ratios in the EMA model are the same according to a simple geometric argument,

$$v_{\text{air}} = v_{\text{substrate}}, \tag{2}$$

estimated as

$$v_{\text{air/substrate}} = \frac{(t_{\text{total}} - 0.35)}{t_{\text{total}}} \frac{1}{2} \times 100\%. \tag{3}$$

The initial thickness t_{total} of the top EMA layer was set to the step height measured by AFM. Both its thickness and compositional parameters were varied in the fitting procedure to account for the variation in the step height or intercalated graphene coverage inhomogeneity throughout the sample.

In this paper we aim to provide a reliable model dielectric function (MDF) of graphene over the entire investigated spectral range. The obtained dispersion can be used to calculate the optical response of graphene-based optoelectronic devices. The proposed MDF is composed of several Kramers-Kronig consistent oscillator terms,

$$\epsilon = \epsilon_\infty + \epsilon_{L1} + \epsilon_G + \epsilon_{L2}, \tag{4}$$

where $\epsilon = \epsilon_1 + i\epsilon_2$. L stands for Lorentz and G for Gaussian oscillators. Adapted variants of these were used in this work. The Lorentz oscillator is defined as

$$\epsilon_{\text{Lorentz}}(E) = \frac{A\gamma E_0}{E_0^2 - E^2 - iE\gamma}, \tag{5}$$

while the Gaussian oscillator as

$$\begin{aligned}\epsilon_{\text{Gaussian}}(E) = A\left[\Gamma\left(\frac{E - E_0}{\sigma}\right) + \Gamma\left(\frac{E + E_0}{\sigma}\right)\right] \\ + iA\left\{\exp\left[-\left(\frac{E - E_0}{\sigma}\right)^2\right]\right. \\ \left. - \exp\left[-\left(\frac{E + E_0}{\sigma}\right)^2\right]\right\},\end{aligned} \tag{6}$$

with

$$\sigma = \frac{\gamma}{2\sqrt{\ln(2)}}. \tag{7}$$

Here, A stands for the amplitude, γ is the broadening parameter, and E_0 is the central energy. The Γ function is a convergence series that produces a Kramers-Kronig consistent line shape for ϵ_1. The term L_1 qualitatively describes the permittivity in the lowest-energy range that is affected by interference oscillations. We thus do not assign a deep

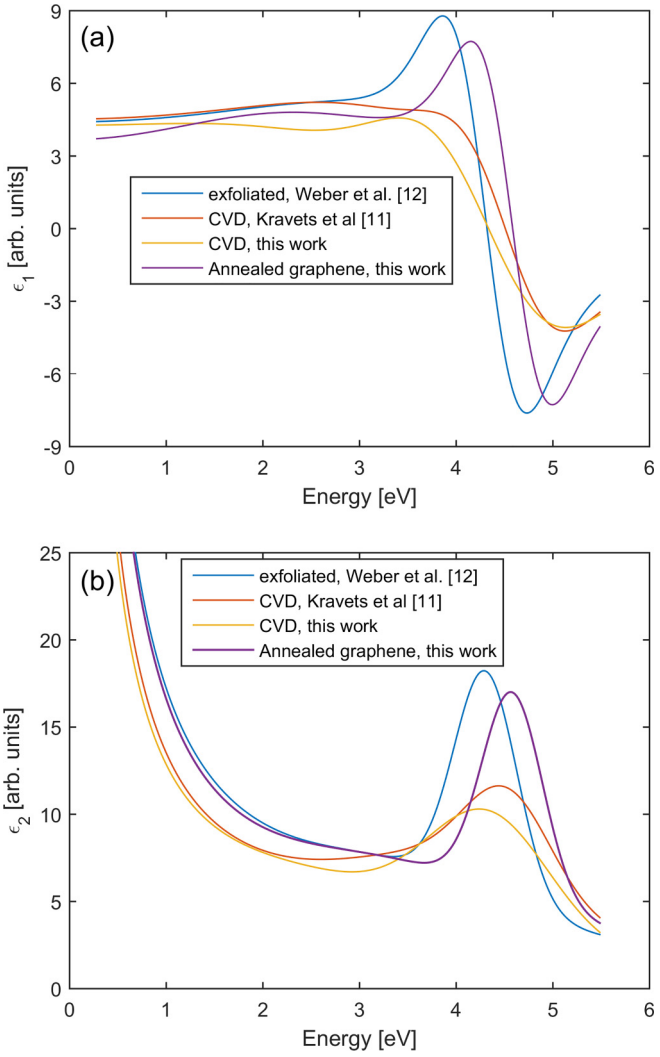

FIG. 4. (a) Real and (b) imaginary parts of the epitaxial graphene dielectric function compared to the literature spectra.

physical interpretation to the fitted parameters of these oscillators. They serve purely to provide the spectral dependence of the MDF. Information about electronic parameters such as relaxation time, etc., could be obtained by other more suitable experimental techniques, e.g., electronic transport measurements or Landau level spectroscopy.

The parameters of these dispersion terms were fit simultaneously with the t_{total} and volume ratios to the ellipsometric experimental data and optical transmission (see Fig. 2). The fit with a mean square error of 14.9 was achieved and the final step height was fitted to be 1.68 nm, close to the initial value of 1.4 nm. Experimental and model spectra of the ellipsometric angles Δ and Ψ are shown in Fig. 2(a), and transmittance in Fig. 2(b). Best-fit MDF parameters are summarized in Table I. The resulting spectral dependence of the dielectric function of monolayer graphene compared to several spectra taken from the literature is shown in Fig. 4. Included in the comparison is the CVD graphene grown on a Si substrate. Its dielectric function was determined similarly by spectroscopic ellipsometry. The explicit tabulated values of the best-fit graphene dielectric function are available in the Supplemental Material [32].

TABLE I. Fitted parameters of spectral dispersion of optical properties of quasi-freestanding graphene monolayer on 6H-SiC.

Oscillator type	Amplitude (arb. units)	γ (eV)	E_0 (eV)
ϵ_∞	2.259		
Lorentz$_1$	16588.6	3.1482	0.001
Gaussian	4.8	4.6778	4.121
Lorentz$_2$	11.7	0.7369	4.581

The fitted spectral dependence of monolayer graphene permittivity (shown in Fig. 4) clearly exhibits a narrow peak located at 4.56 eV. This energy corresponds to the critical point associated with the van Hove singularity in the joint density of states. It is related to the interband transitions between π-π^* hybridized orbitals in the vicinity of the M point of the graphene Brillouin zone. Several reports have shown that in multilayer graphene systems, the position and appearance of multiple van Hove singularities can be tailored by twisting individual graphene layers, dramatically increasing the light-matter interaction [33–35].

The main peak of the investigated sample is comparably as narrow as in exfoliated graphene, yet blueshifted as in CVD graphene. When comparing the optical properties of the investigated sample with exfoliated graphene, one can see that the transition energy near the M point in the investigated sample is slightly increased, which might be a consequence of the changes induced in the lattice during graphitization and step bunching. However, carbon covalent sp bonds are known to be very strong and robust, rendering this option unlikely. In the single-particle picture, the maximum of the absorption is theoretically expected around 5.1–5.2 eV [36]. Depending on the substrate and doping, the Coulomb interaction in graphene may remain, to a great extent, unscreened. This allows the charge interaction to take place. When excitonic effects and the electron-electron interaction are taken into account [11,34–36], they suppress and redshift the peak which is observable in pristine exfoliated and CVD graphene samples. In a freestanding graphene, the shift has a well-defined value of ∼600 meV, down to 4.5–4.6 eV [11,36–38]. For bilayer graphene, the redshift is even stronger, ∼800 meV in Ref. [39]. The peak shifts further with an increasing number of layers, eventually reaching the known graphite value of 4.5 eV. Apparently, the peak position also depends on the polymorph of the SiC substrate, as was indicated in a report examining epitaxial graphene grown on Si-face 3C and Si-/C-face 4H. There is a clear indication showing that the peak in ϵ_2 tends to shift below 4.5 eV in the C-face and to higher energy in the Si-face case [Fig. 5(a) [19]]. Besides that, there is an inverse dependence between the substrate annealing temperature and the peak position, as was shown by examining graphene produced on the C-face 4H substrate [Fig. 5(b) [22]]. In this regard, our findings would be consistent with the reports, in particular concerning the Si face on which the graphene was grown. On the other hand, intercalation should suppress bonding with the substrate. The blueshift might be related to the effect of intercalation itself. As a matter of fact, the charge carriers present in the substrate may lead to screening between graphene and the substrate material. The

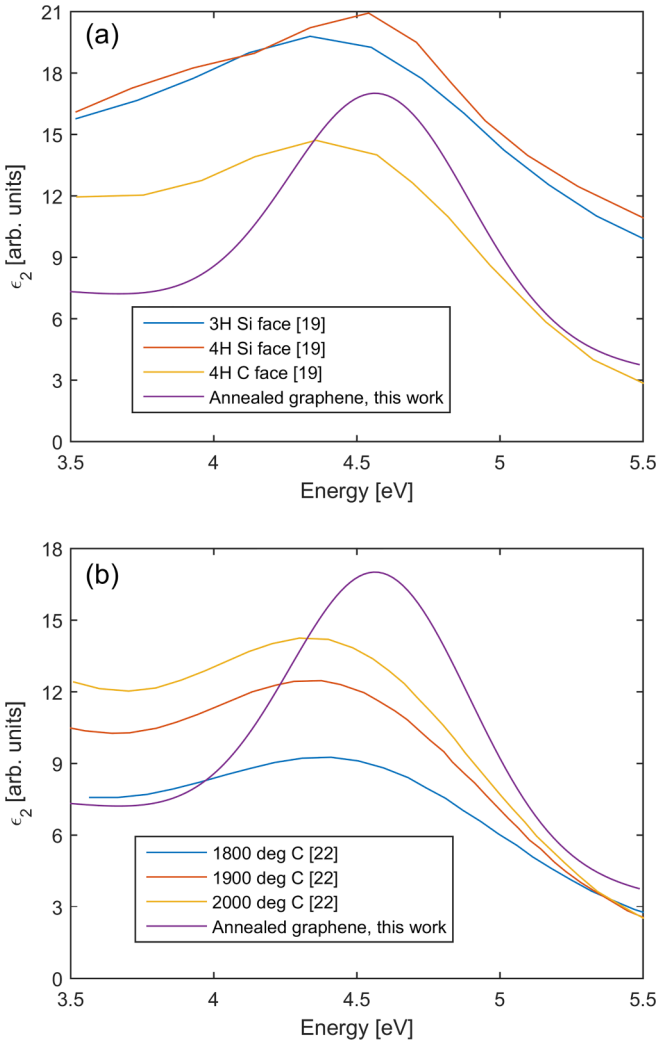

FIG. 5. The imaginary part of the dielectric function in the region of the 4.5 eV peak for several polymorphs of SiC (a) and for the C-face 4H-SiC annealed at various temperatures complemented by the spectra of annealed graphene obtained in this work (b).

distinction is evident when comparing insulating and conducting substrates such as silicon/quartz versus copper. In samples with metallic substrates, the shift of the peak, as compared to the single-particle prediction, is weaker, yielding a peak energy of 4.8–4.9 eV. Screening also affects the peak shape: Without any, the peak is asymmetric with a higher value below the critical point; with a high degree of screening, the peak becomes more symmetric [14,40]. The sharpness of the peak thus confirms the good quality of our sample. Even though intercalation reduces bonding between the layers, hydrogen atoms close to graphene might induce electrostatic interactions and doping of graphene layer, resulting in the blueshift.

To make a better comparison with the literature in terms of optical conductivity, we calculated the real part of sheet

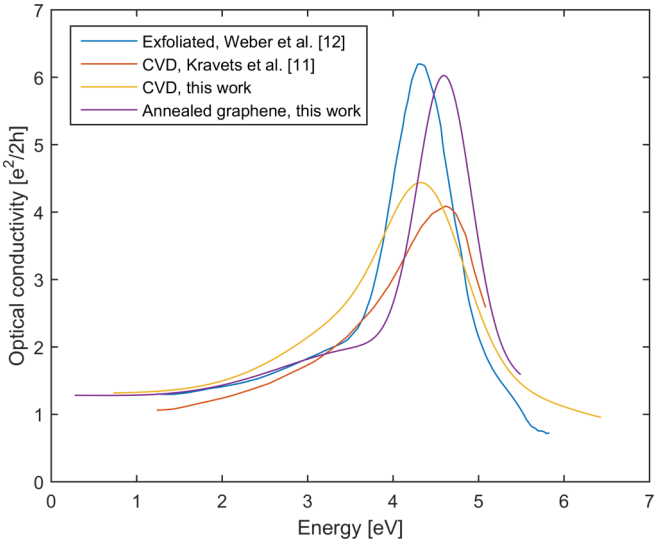

FIG. 6. Real part of the optical conductivity of epitaxial graphene and its comparison with other types of graphene.

optical conductivity. It reveals an additional fundamental feature of graphene. Namely, it should exhibit a universal value of conductivity $\sigma_0 = e^2/2h$ at IR energies [41,42]. In Fig. 6, we compare the resulting optical conductivity with two cases from the literature, exfoliated [12] and CVD graphene [13], as well as the CVD sample. Apart from higher conductivity values at UV energies arising from interband transitions, the conductivity of the investigated sample approaches unity and closely resembles exfoliated graphene at energies below 3 eV.

V. CONCLUSION

We have characterized the dielectric function of intercalated epitaxial monolayer graphene grown on 6H-SiC. The overall spectral dependence of the dielectric function from infrared to visible energies, narrowness and the magnitude of the main peak, and approaching the universal value of optical conductivity at IR energies allows us to conclude that annealing and intercalation of the (0001) surface of 6H-SiC allows us to produce large-area excellent quality graphene monolayers. The investigated sample is very close to those prepared by exfoliation from the optical point of view. The spectral dependence of optical constants can be utilized in the theoretical design of nano-optoelectronic devices with graphene working in a broad spectral range.

ACKNOWLEDGMENT

This work was supported by Czech Ministry of Education, Youth and Sports, program MOBILITY (Grant No. 8J22FR006).

[1] K. S. Novoselov, A. K. Geim, S. V. Morozov, D. Jiang, Y. Zhang, S. V. Dubonos, I. V. Grigorieva, and A. A. Firsov, Electric field effect in atomically thin carbon films, Science **306**, 666 (2004).

[2] K. I. Bolotin, K. J. Sikes, Z. Jiang, M. Klima, G. Fudenberg, J. Hone, P. Kim, and H. L. Stormer, Ultrahigh electron mobility in suspended graphene, Solid State Commun. **146**, 351 (2008).

[3] C. R. Dean, A. F. Young, I. Meric, C. Lee, L. Wang, S. Sorgenfrei, K. Watanabe, T. Taniguchi, P. Kim, K. L. Shepard *et al.*, Boron nitride substrates for high-quality graphene electronics, Nat. Nanotechnol. **5**, 722 (2010).

[4] K. F. Mak, C. H. Lui, J. Shan, and T. F. Heinz, Observation of an Electric-Field-Induced Band Gap in Bilayer Graphene by Infrared Spectroscopy, Phys. Rev. Lett. **102**, 256405 (2009).

[5] K. J. Tielrooij, L. Piatkowski, M. Massicotte, A. Woessner, Q. Ma, Y. Lee, K. S. Myhro, C. N. Lau, P. Jarillo-Herrero, N. F. van Hulst *et al.*, Generation of photovoltage in graphene on a femtosecond timescale through efficient carrier heating, Nat. Nanotechnol. **10**, 437 (2015).

[6] I. Khrapach, F. Withers, T. H. Bointon, D. K. Polyushkin, W. L. Barnes, S. Russo, and M. F. Craciun, Novel highly conductive and transparent graphene-based conductors, Adv. Mater. **24**, 2844 (2012).

[7] H. Kinoshita, I. Jeon, M. Maruyama, K. Kawahara, Y. Terao, D. Ding, R. Matsumoto, Y. Matsuo, S. Okada, and H. Ago, Highly Conductive and transparent large-area bilayer graphene realized by $MoCl_5$ intercalation, Adv. Mater. **29**, 1702141 (2017).

[8] J. Zhou, Z. Ren, S. Li, Z. Liang, C. Surya, and H. Shen, Semi-transparent Cl-doped perovskite solar cells with graphene electrodes for tandem application, Mater. Lett. **220**, 82 (2018).

[9] K. S. Novoselov, A. K. Geim, S. V. Morozov, D. Jiang, M. I. Katsnelson, I. V. Grigorieva, S. V. Dubonos, and A. A. Firsov, Two-dimensional gas of massless Dirac fermions in graphene, Nature (London) **438**, 197 (2005).

[10] A. Gray, M. Balooch, S. Allegret, S. D. Gendt, and W.-E. Wang, Optical detection and characterization of graphene by broadband spectrophotometry, J. Appl. Phys. **104**, 053109 (2008).

[11] V. G. Kravets, A. N. Grigorenko, R. R. Nair, P. Blake, S. Anissimova, K. S. Novoselov, and A. K. Geim, Spectroscopic ellipsometry of graphene and an exciton-shifted van Hove peak in absorption, Phys. Rev. B **81**, 155413 (2010).

[12] J. W. Weber, V. E. Calado, and M. C. M. van de Sanden, Optical constants of graphene measured by spectroscopic ellipsometry, Appl. Phys. Lett. **97**, 091904 (2010).

[13] F. J. Nelson, V. K. Kamineni, T. Zhang, E. S. Comfort, J. U. Lee, and A. C. Diebold, Optical properties of large-area polycrystalline chemical vapor deposited graphene by spectroscopic ellipsometry, Appl. Phys. Lett. **97**, 253110 (2010)

[14] M. Losurdo, M. M. Giangregorio, G. V. Bianco, P. Capezzuto, and G. Bruno, How spectroscopic ellipsometry can aid graphene technology?, Thin Solid Films **571**, 389 (2014).

[15] O. Fursenko, M. Lukosius, G. Lupina, J. Bauer, C. Villringer, and A. Mai, Development of graphene process control by industrial optical spectroscopy setup, Proc. SPIE **10330**, 1033017 (2017).

[16] F. Speck, J. Jobst, F. Fromm, M. Ostler, D. Waldmann, M. Hundhausen, H. B. Weber, and Th. Seyller, The quasi-free-standing nature of graphene on H-saturated SiC(0001), Appl. Phys. Lett. **99**, 122106 (2011)

[17] C. Riedl, C. Coletti, T. Iwasaki, A. A. Zakharov, and U. Starke, Quasi-Free-Standing Epitaxial Graphene on SiC Obtained by Hydrogen Intercalation, Phys. Rev. Lett. **103**, 246804 (2009).

[18] K. V. Emtsev, A. Bostwick, K. Horn, J. Jobst, G. L. Kellogg, L. Ley, J. L. McChesney, T. Ohta, S. A. Reshanov, J. Rohrl *et al.*, Towards wafer-size graphene layers by atmospheric pressure graphitization of silicon carbide, Nat. Mater. **8**, 203 (2009).

[19] A. Boosalis, T. Hofmann, V. Darakchieva, R. Yakimova, and M. Schubert, Visible to vacuum ultraviolet dielectric functions of epitaxial graphene on 3C and 4H SiC polytypes determined by spectroscopic ellipsometry, Appl. Phys. Lett. **101**, 011912 (2012).

[20] I. Santoso, S. I. Santoso, S. L. Wong, X. Yin, P. K. Gogoi, T. C. Asmara, H. Huang, W. Chen, T. S. Wee, and A. Rusydi, Optical and electronic structure of quasi-freestanding multilayer graphene on the carbon face of SiC, Europhys. Lett. **108**, 37009 (2014).

[21] R. Yakimova, T. Iakimova, G. R. Yazdi, C. Bouhafs, J. Eriksson, A. Zakharov, A. Boosalis, M. Schubert, and V. Darakchieva, Morphological and electronic properties of epitaxial graphene on SiC, Phys. B: Condens. Matter **439**, 54 (2014).

[22] C. Bouhafs, V. Darakchieva, I. L. Persson, A. Tiberj, P. O. Persson, M. Paillet, A.-A. Zahab, P. Landois, S. Juillaguet, S. Schöche *et al.*, Structural properties and dielectric function of graphene grown by high-temperature sublimation on 4H-SiC(000-1), J. Appl. Phys. **117**, 085701 (2015).

[23] F. Nelson, A. Sandin, D. B. Dougherty, D. E. Aspnes, J. E. Rowe, and A. C. Diebold, Optical and structural characterization of epitaxial graphene on vicinal 6H-SiC(0001)-Si by spectroscopic ellipsometry, Auger spectroscopy, and STM, J. Vac. Sci. Technol. B **30**, 04E106 (2012).

[24] F. Speck, M. Ostler, S. Besendörfer, J. Krone, M. Wanke, and T. Seyller, Growth and intercalation of graphene on silicon carbide studied by low-energy electron microscopy, Ann. Phys. **529**, 1700046 (2017).

[25] G. Yazdi, T. Iakimov, and R. Yakimova, Epitaxial graphene on SiC: A review of growth and characterization, Crystals **6**, 53 (2016).

[26] S. Ninomiya and S. Adachi, Optical constants of 6H-SiC single crystals, Jpn. J. Appl. Phys. **33**, 2479 (1994).

[27] C. Xie, P. Xu, F. Xu, H. Pan, and Y. Li, First-principles studies of the electronic and optical properties of 6H-SiC, Phys. B: Condens. Matter **336**, 284 (2003).

[28] K.-H. Lee, C. H. Park, B.-H. Cheong, and K. J. Chang, First-principles study of the optical properties of SiC, Solid State Commun. **92**, 869 (1994).

[29] B. Adolph, K. Tenelsen, V. I. Gavrilenko, and F. Bechstedt, Optical and loss spectra of SiC polytypes from *ab initio* calculations, Phys. Rev. B **55**, 1422 (1997).

[30] S. Zollner, J. G. Chen, E. Duda, T. Wetteroth, S. R. Wilson, and J. N. Hilfiker, Dielectric functions of bulk 4H and 6H SiC and spectroscopic ellipsometry studies of thin SiC films on Si, J. Appl. Phys. **85**, 8353 (1999).

[31] O. P. A. Lindquist, K. Järrendahl, H. Arwin, S. Peters, J.-T. Zettler, C. Cobet, N. Nesser, D. E. Aspnes, A. Henry, and N. V. Edwards, Ordinary and extra-ordinary dielectric functions of 4H- and 6H-SiC in the 0.7 to 9.0 eV photon energy range, Mater. Res. Soc. Symp. Proc. **640**, H5.24 (2001).

[32] See Supplemental Material at http://link.aps.org/supplemental/10.1103/PhysRevMaterials.7.044201 for the explicit tabulated values of the best-fit quasi-freestanding epitaxial graphene dielectric function.

[33] G. Li, A. Luican, J. M. B. Lopes dos Santos, A. H. Castro Neto, A. Reina, J. Kong, and E. Y. Andrei, Observation of Van

Hove singularities in twisted graphene layers, Nat. Phys. **6**, 109 (2010).

[34] R. W. Havener, Y. Liang, L. Brown, L. Yang, and J. Park, Van Hove singularities and excitonic effects in the optical conductivity of twisted bilayer graphene, Nano Lett. **14**, 3353 (2014).

[35] J. Yin, H. Wang, H. Peng, Z. Tan, L. Liao, L. Lin, X. Sun, A. L. Koh, Y. Chen, H. Peng *et al.*, Selectively enhanced photocurrent generation in twisted bilayer graphene with van Hove singularity, Nat. Commun. **7**, 10699 (2016).

[36] L. Yang, J. Deslippe, C.-H. Park, M. L. Cohen, and S. G. Louie, Excitonic Effects on the Optical Response of Graphene and Bilayer Graphene, Phys. Rev. Lett. **103**, 186802 (2009).

[37] K. F. Mak, J. Shan, and T. F. Heinz, Seeing Many-Body Effects in Single- and Few-Layer Graphene: Observation of Two-Dimensional Saddle-Point Excitons, Phys. Rev. Lett. **106**, 046401 (2011).

[38] D.-H. Chae, T. Utikal, S. Weisenburger, H. Giessen, K. v. Klitzing, M. Lippitz, and J. Smet, Excitonic Fano Resonance in Free-Standing Graphene, Nano Lett. **11**, 1379 (2011).

[39] Y.-C. Chang, C.-H. Liu, C.-H. Liu, Z. Zhong, and T. B. Norris, Extracting the complex optical conductivity of mono- and bilayer graphene by ellipsometry, Appl. Phys. Lett. **140**, 261909 (2014).

[40] P. K. Gogoi, I. Santoso, S. Saha, S. Wang, A. H. Castro Neto, K. P. Loh, T. Venkatesan, and A. Rusydi, Optical conductivity study of screening of many-body effects in graphene interfaces, Europhys. Lett. **99**, 67009 (2012).

[41] L. A. Falkovsky and A. A. Varlamov, Space-time dispersion of graphene conductivity, Eur. Phys. J. B **56**, 281 (2007).

[42] T. Stauber, N. M. R. Peres, and A. K. Geim, Optical conductivity of graphene in the visible region of the spectrum, Phys. Rev. B **78**, 085432 (2008).